HYDROLOGICAL RESPONSES TO THE SYNERGISTIC CHANGES IN CLIMATE AND LAND COVER IN THE ALPINE PASTORAL REGION

BY

MINGYUE XIE

THESIS

Submitted in partial fulfillment of the requirements
for the degree of Master of Science in Civil Engineering
in the Graduate College of the
University of Illinois Urbana-Champaign, 2021

Urbana, Illinois

Adviser:

Professor Ximing Cai

ABSTRACT

Quantifying the hydrological responses to climate change and land use and land cover (LULC) change is imperative for sustainable river basin management. In this study, hydrological regimes of the upper Lancang River Basin under environmental changes are assessed using a semi-distributed hydrologic model, Soil and Water Assessment Tool (SWAT). The non-parametric test is used to analyze the trend of hydro-meteorological variables based on the hydro-meteorological data time series analysis during the period of 1978 - 2014. Global Climate Models (or General Circulation Model, GCMs) under RCP 4.5 is used to assess the future climate (2021-2080); future hypothetical land-use change (2040) is predicted by Land Change Modeler (LCM). The modelling results are evaluated in four scenarios: scenario 1 with historical land use and climate, scenario 2 with the current land use and climate data from the past, scenario 3 with the current land use map and future climate, and scenario 4 with future land use and future climate. Consequently, sediment yield rises by 5.0 %, 17.9 %, and 25.9 % under scenarios 2, 3, and 4, respectively, as compared to scenario 1. The results indicate that the transition from pasture to cropland has been the topmost contributor to the increase in runoff and sediment yield, which is likely to continue to the future. Additionally, climate and land use change have a larger synergistic influence than their separate effects. This study quantitatively assesses the hydrological responses to environmental changes in an alpine pastoral area and provides supports for sustainable river basin management.

ACKNOWLEDGMENTS

The accomplishment of the work is attributed to the support from many people. I would like to express my gratitude to my adviser, Professor Ximing Cai, for his continuous support and advice. His critical insights and invaluable guidance to help me initiate, improve, and finalize the thesis. It is a great honor to work under his authoritative supervision. I also would like to thank my co-advisor, Prof. Yu Li, for the suggestions. His in-depth knowledge and abundant experience of the study site are meant to solve the issues, especially with the data, in the research. Their meticulous scrutiny and scientific advice have helped me a lot to accomplish the work. Besides, I am also grateful to the students from Prof Cai's group for their feedback and suggestions.

Finally, I thank my family and friends for their unconditional trust, encouragement, and mental support with patience.

TABLE OF CONTENTS

CHAPTER 1: Introduction

Climate change and land use and land cover (LULC) change are the two principal drivers of hydrological regimes and significantly influence the hydrological characteristics in many river basins. Climate variables, such as precipitation, temperature, wind speed, and humidity, determine the hydrological cycle's major inputs and change the hydrological system. Specifically, climate change is a critical factor determining hydrological processing, including both runoff and sediment loads, by changing the spatial and temporal distribution of precipitation and temperature. Such hydrological changes vary by region around the globe. In recent decades, with climate change, the hydrological processes have undergone considerable changes, affecting the spatiotemporal distribution of water resources.

Land use and land cover has experienced transformation under climate change and human interference in many regions (Xu et al., 2008; Wang et al., 2015; Bunting et al., 2016; Zarei et al., 2020). LULC changes, including the vegetation type alterations, land use practices transitions and their spatial patterns, bring up effects on watershed hydrological processing by affecting evapotranspiration (ET), soil infiltration capacity, surface, and subsurface flow regimes, and ultimately affecting the availability of water resources in a river basin (Brown et al., 2005; Romanowicz and Booij, 2011; Cuo et al., 2013). Quantifying hydrological responses to climate change and LULC change is critical to river basin planning and management and ecosystem restoration.

Watershed hydrology alterations under environmental changes have been extensively studied during the past decades. Climate change, resulting from the enhanced greenhouse effect, has been recognized as the primary driver of watershed hydrology. The previous studies demonstrated that hydrological processing had a dynamic response to the change of meteorological factors (Amisigo et al., 2015). For example, Legesse et al. (2003) assessed streamflow responses to land-use changes and climatic variability using the distributed Precipitation Runoff Modelling System (PRMS) in the Ketar River Basin, confirming that increasing air temperature results in a decrease in catchment discharge. Additionally, some studies have found that increased rainfall intensity contributes to increased sediment loads in various river basins. Awotwi et al. (2015a) investigated the effects of climatic variability on water balance components using the SWAT model in the White Volta basin. They verified that increases in precipitation and temperature enhanced in surface runoff, base flow, and evapotranspiration. Dibaba et al. (2020) identified the

decline of annual flow due to climate change effects; as a result, the study found that water availability would be reduced in the upper Blue Nile Basin under future climate scenario.

Changes in land use and land cover characteristics have given rise to hydrological responses changes over the past decades (Hu et al., 2005). Albhaisi et al. (2013) demonstrated a systematic increase in groundwater recharge resulted from LULC change in the Upper Berg catchment, South Africa. Mengistu (2009) used SWAT and Hydrological Simulation Program – FORTRAN (HSPF) models to quantify the hydrological responses to LULC change at Hare Watershed, Ethiopia; the analysis revealed that the change of land use pattern altered the hydrological cycle, leading to an increase in runoff. Land use practices transition and land cover degradation also make the soils more vulnerable to erosion and increase flood frequency. Bonell et al. (2010), for example, indicated that the removal of vegetation followed by land-use practices transition might compact soils and accelerate soil erosion. Awotwi et al. (2015b) showed a link between land cover and the hydrologic response, demonstrating that conversion of savannah and grassland to farmlands increased evapotranspiration while decreasing surface flow.

Climate changes bring out significantly impacts on land use and land cover, as well as hydrological processing. In the coupled system, the synergy between climate change and vegetation cover is necessary to assure the dependability of results. Zarei (2020) developed a correlation between the vegetation index and climate variables using regression equations established between satellite data images and data obtained from weather stations. Consequently, it is a trend to study the influence of vegetation driven by climate change rather than only consider the direct impact of climate variation. Numerous studies have been carried out worldwide examining the relationship between hydrological processing and synergistic changes of climate and LULC. For instance, Mango et al. (2011) conducted a large-scale study to evaluate the impacts of combined climate and LULC changes on hydrological responses in the upper Mara River in Africa using SWAT. Guo et al. (2008) examined LULC and climate change effects on temporal variation of streamflow in the Poyang Lake basin. Xu et al. (2014) According to Xu et al. (2014), the consequences of climate change and LULC change are responsible for a runoff drop of 26.9 % and 73.1 %, respectively. Shrestha (2018) compared the combined and individual impacts of climate change and changes in vegetation cover on runoff and sediment yield. Zhang et al. (2019) developed a SWAT model and showed that the synergetic effects enhance the average annual runoff by 15% to 38% relative to the base period.

The physically based hydrological model and the elasticity method based on the Budyko hypothesis are commonly used to assess the variability of the watershed hydrological cycle under different environmental scenarios. Physically based distributed hydrological models can consider spatial and temporal heterogeneity and describe natural processing more precisely than conceptual models (Finger et al., 2011). As a result, the modelling approach is widely applied due to its superiorities. For example, the SWAT model has been extensively utilized to simulate and forecast hydrological processes in many river basins (Arnorld et al., 1998; Jayakrishnan et al., 2005; Briak et al., 2016).

As an alpine pastoral region and a unique ecological zone, the upper Lancang river basin (LRB) has experienced dramatic changes in hydrological processing caused by continuous climate and LULC change. The primary vegetation cover type is grassland, which growth is more sensitive to climate change than other vegetation types. Consequently, alpine pastoral regions are especially vulnerable and susceptible to the worst manifestations of climate change, including severe soil loss rates (Orlandi et al., 2016). In addition, a significant portion of natural runoff is driven by snowmelt in these regions, which indicates that the temperature can directly determine the timing of snowmelt runoff. As a result, LULC conversions driven by climate change may aggravate the unignorable ill effects of climate change. For example, as the world's largest alpine pastoral region, the warming and wetting of the climate have favored vegetation growth directly in Tibetan Plateau over the past decades (Wei et al., 2020; Tian et al., 2020). Rostamian et al. (2008) applied SWAT to estimate runoff and sediment yield and assessed the model’s performance in two mountainous basins in central Iran that are mostly covered by pasture and cropland. Yang et al. (2017) used SWAT to investigate the distinct impacts of climatic and land cover on flow regime changes in Yingluoxia and Minxian catchments; the findings indicated that climatic factors indeed dominated flow regime changes on the Northeastern Tibetan Plateau. It is critical to analyze the dynamic responses of hydrological processing to synergistic climate and LULC change in the alpine pastoral region.

This study aims to take a comprehensive perspective to analyze the synergistic impacts of climatic and LULC changes on watershed hydrology. A calibrated and validated physically based SWAT hydrological model is used to simulate the hydrological regimes. GCMs and LCM are used to predict future climate and LULC scenarios, respectively. Trend analysis and three precipitation indices are employed to evaluating the change of environmental variables. The study quantifies

the hydrology responses by performing a hydrological model under four scenarios. In summary, the purpose of this study is to investigate the environmental change patterns, reveal the hydrological responses to the synergistic changes in climate and LULC, and provide scientific supports for ecological restoration and sustainable water resources planning and management under future climate change.

CHAPTER 2: Study Area and Data

The sampling site of this study is the upper Lancang River Basin (LRB), which lies upstream of the Lancang-Mekong River. The Lancang River originates from the Qinghai-Tibetan Plateau. The upper LRB has a total area of 52,508 km^2 and an elevation of more than 3000 m (Figure 2.1). The upper LRB has a temperate plateau climate with an average temperature of 10 °C and average annual precipitation of 404.81 mm. The wet season occurs from May to October, which accounts for more than 80% of the annual precipitation.

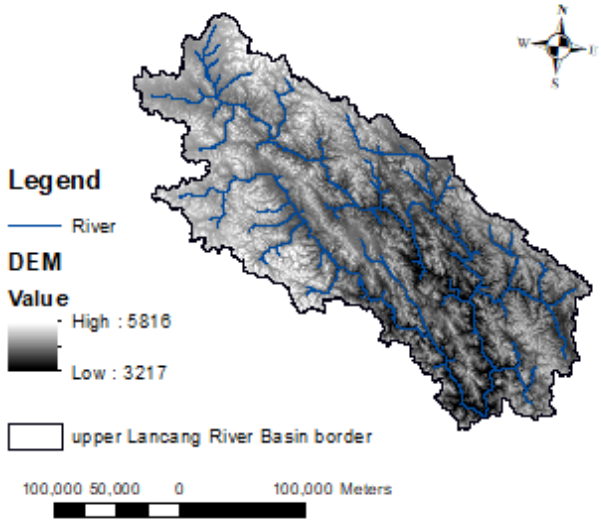

Figure 2.1 Digital elevation model (DEM) in the upper LRB

As a representative alpine pastoral region, LULC has experienced substantial transformation in recent years. Land use and land cover data were collected from European Space Agency from 1992 to 2015 (Figure 2.2). To fit the SWAT model, the original LULC map was reclassified into seven categories: pasture (PAST), forest (FRST), barren land (BARR), water areas (WATR), urban land (URHD), rice (RICE) and wheat (WWHT). The primary land use types are pasture and forest, which account for 83.0% and 5.0% of the total basin area, respectively. According to Figure 2.2, forest is concentrated in the lower middle part of the basin. Crop cultivation and livestock production dominate the local economy in the basin. In the past decades, global warming has led to shrub encroachment in grassland and provided more favorable climatic conditions for crop cultivation in the alpine region. As a result, many herders have chosen to cultivate rather than graze because of climate change and policy implementation. According to the local statistics yearbook, the cultivated land area has increased by an average of 8906.26 km^2/year

during the past 20 years (Table 2.1). However, the number of livestock production has declined in recent years.

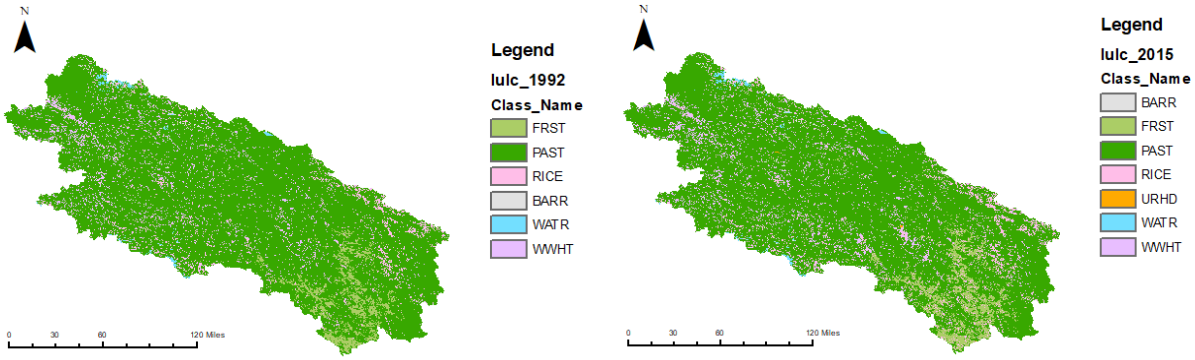

Figure 2.2 Land use map for 1992 and 2015 in the upper LRB.

Table 2.1: Number of Livestock & Area of Cultivated Land in cities within the upper LRB.

Year	Number of Livestock (1000)	Cultivated Land (1000 hectares)
1995	556	354
2000	537	345
2005	557	373
2010	530	368
2015	369	273
2019	276.6	220.9

Table 2.2 summarizes the data used in the research. To set up SWAT model, the Digital Elevation Model (DEM) data was derived from the Geospatial Data Cloud at a 90m resolution ratio. The DEM map is used to generate the slope map and delineate the subbasins for SWAT simulation. Furthermore, the SWAT model requires physical and hydrological properties of soils. The soil map (1:1,000,000) was obtained from the soil databases that was produced by the Nanjing Institute of Soil Science. Daily meteorological data during the period from 1978 to 2014 was collected from China Meteorological Administration.

Table 2.2: Description of research data used in the research.

Data	**Resolution/Time**	**Data Source**
Digital Elevation Model (DEM)	90m×90m	Geospatial Data Cloud
Land use	200m; 1992-2015	European Space Agency
Soil Map	1:1,000,000	Nanjing Institute of Soil Science; Chinese soil database; SPAW software
River Networks	1:250,000	Chinese Academy of Sciences
Daily Meteorological data	33 stations; 1978-2014	China Meteorological Administration (Rainfall, temperature, relative humidity, and solar radiation)
Monthly streamflow	3 stations; 1980–2008	Hydrological statistical yearbook of the Lancang River Basin, and the operating agency of the reservoirs
Monthly transported sediment	3 stations; 1980–1986	Hydrological statistical yearbook of the Lancang River Basin
Normalized Difference Vegetation Index (NDVI)	500m; 1-day	Moderate Resolution Imaging Spectroradiometer (MODIS) images
Cultivated land area	1995-2019	Statistical Yearbook of provinces locating in the basin (Tibet and Qinghai)
Livestock production	1995-2019	Statistical Yearbook of provinces locating in the basin (Tibet and Qinghai)

CHAPTER 3: Methodology

3.1 Hydrological Model

SWAT is a comprehensive, semi-distributed, and physically based tool developed by the United States Department of Agriculture (USDA) that can be used to tackle hydrological and environmental problems at different catchment scales (Novotny et al., 2007; Arnold et al., 2012; Aboelnour et al., 2020). SWAT has been widely used to model the impact of land management practices on water, sediment and agricultural chemical yields. The model components can describe processing associated with water movement, sediment movement, soils, weather, plant growth, nutrients cycling and land management (Srinivasan et al., 1998; Gassman et al., 2014; Yesuf, 2015; Trang et al., 2017). In this study, a SWAT model is developed to perform long-term continuous simulation of hydrological processing under different scenarios in the upper LRB.

In this model, the upper LRB is delineated into 150 sub-basins. The sub-basins are further divided into 958 hydrological response units (HRUs) depending on land use, soil type and slope. The SWAT model estimates the surface runoff volumes from daily rainfall within each HRU using a modified Soil Conservation Service curve number (SCS-CN) approach (USDA Soil Conservation Service, 1972). The CN (dimensionless number ranging from 0 to 100) depends on soil group, land use, and management practice. Erosion and sediment yield are estimated for each sub-basin using the Modified Universal Soil Loss Equation (MUSLE) developed by Williams and Brendt (1977). The SWAT model in this study simulates both streamflow and sediment yield.

3.2 Scenario Design

To quantitatively analyze the impacts of environmental factors on the hydrological processing, four experiments were conducted under various scenarios. They are the combinations of climate and LULC data (Table 3.1): scenario 1 with historical land use and historical climate, scenario 2 with current land use and historical climate, scenario 3 with current land use and future climate, and scenario 4 with future land use and future climate. By comparing simulation results between scenarios, the impacts of two environmental factors on hydrological processing can be quantitatively analyzed throughout time.

Table 3.1: Scenario design for SWAT model.

Scenarios	Climate data	Land use data
1	1978 - 2014	LULC 1992
2	1978 - 2014	LULC 2015
3	2021 – 2080	LULC 2015
4	2021 - 2080	LULC 2040

3.2.1 Climate Change Projection

To investigate the climate change impacts on watershed hydrology, the common methodology is to introduce the outputs General Circulation Models (GCMs) into the hydrological models (Gosling et al., 2011). The Coupled Model Intercomparison Project Phase 5 (CMIP5) generated a multi-model dataset of projected global climatic changes. CMIP5 includes 40 GCMs, and its outputs include historical climate simulations from 1850 to 2005, as well as climate projection for the near term (up to around 2035) and long term (up to 2100 and beyond) based on four Representative Concentration Pathways (RCPs) (Kamworapan et al., 2019). The coupled general circulation model (CM3) developed by the Geophysical Fluid Dynamics Laboratory (GFDL) is beneficial for addressing the climate change concerns (Donner et al., 2011, Griffies et al., 2011). In this study, GFDL-CM3 for the CMIP5 is employed to generate future climatic variables under RCP 4.5 emission scenario.

Daily climatic datasets over the coming 60 years (2021-2080), including maximum and minimum temperature and precipitation, are derived from CMIP5 at $2.5° \times 2°$ resolution. Furthermore, the results statistically downscaled to a resolution of $0.5° \times 0.5°$. Because the future climate datasets are projected on a grid-scale, the inverse distance weighting (IDW) method is used to interpolate the spatial climatic data into 33 weather stations around the river basin to serve as climate inputs of the hydrological model.

3.2.2 LULC Change Projection

Land Change Modeler (LCM) is an integrated software developed by IDRISI Selva (Adhikari and Southworth, 2012). In this study, LCM is used to analyze the trend of LULC change for different classes amid 1992-2015 and predict the land use map for the year 2040. The LULC change simulation and forecast are done on a neural network built-in module, which can be used to incorporate spatial interaction and stimulate LULC categories (Mishra et al., 2014; Jain et al.,

2017). LULC transitions are modelled using the Multi-Layer Perceptron (MLP) neural network. Transition potential represents the relative potential of land to go through each of the transitions. Based on the transition matrix, LCM analyzes land use change over the historical period to determine the expected quantity of pixels that went through the transition being modified and determine the spatial allocation of the change pixels using the previous (1992) and later (2015) LULC maps.

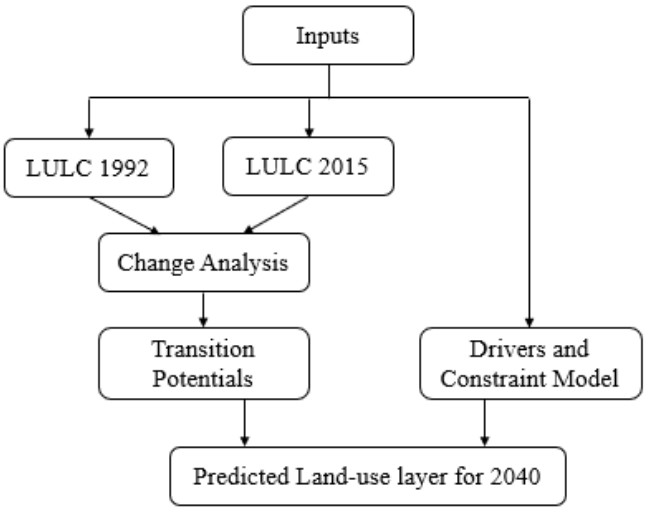

Figure 3.1 Schematic diagram of the methodology flow chart for LCM.

3.3 Statistics Analysis

3.3.1 Mann-Kendall (M-K) Test

The Mann-Kendall (M-K) test is a non-parametric rank-based test used for detecting monotonic trend (Mann, 1945; Kendall, 1975). The M-K test can identify a trend in a time series without specifying whether the trend is linear or non-linear (Khaliq et al., 2009). Numerous studies have used the M-K test to assess the spatial and temporal trends in the hydro-climatic time series (e.g., Zhang et al. 2004; Ahmad et al., 2o15; Gebremicael et al., 2013). In this paper, the M-K test is conducted to analyze the variation in meteorological and hydrological components during historical and future periods.

The M-K statistics (S) is defined as

$$S = \sum_{i=1}^{N-1} \sum_{j=i+1}^{N} sgn(x_j - x_i) \quad (1)$$

with

$$sgn(x_y - x_i)\begin{cases}1 & if\ x_j - x_i > 1\\ 0 & if\ x_j - x_i = 1\\ -1 & if\ x_j - x_i < 1\end{cases} \quad (2)$$

where N is the length of time series, x_i and x_j are the time series observations in chronological order.

The variance for the statistics S is defined by

$$V(S) = \frac{1}{18}\left[N(N-1)(2N+5) - \sum_{p=1}^{q} t_p(t_p - 1)(2t_p + 5)\right] \quad (3)$$

where t_p is the number of data points in the pth tied group and q is the number of tied groups. The normalized test statistics Z for the M-K test is computing using the equation below:

$$Z = \begin{cases}\dfrac{S-1}{\sqrt{VAR(S)}} & if\ S > 0\\ 0 & if\ S = 0\\ \dfrac{S+1}{\sqrt{VAR(S)}} & if\ S < 0\end{cases} \quad (4)$$

Z follows up a standard normal distribution (Adamowski and Bougadis 2003). Positive Z values indicate an upward trend in the hydrologic time series, while negative values show a decreasing trend. Additionally, a two-tailed probability (p-value) will be computed to identify the trend of variables. A statistical significance level α is also defined to identify the trend of variables. The null hypothesis of no trend is rejected if the absolute value of Z is greater than the theoretical value $Z_{1-\alpha/2}$ (Pingale et al. 2016).

3.3.2 Precipitation Concentration Index (PCI)

The variation of precipitation concentration plays a decisive role in hydrological processing (Ezenwaji et al., 2017). The Precipitation Concentration Index (PCI) is an effective indicator of the temporal inhomogeneity of precipitation and widely used to evaluate the seasonal variability of precipitation (e.g., Michiels et al., 1992; Luis et al., 2011). This study conducts a frequency analysis of rainfall series using the precipitation heterogeneity index to analyze the variations of precipitation concentration on an annual scale.

To assess the effects of the contribution of the days with the most significant rainfall to the total amount, the cumulative percentage of precipitation (Y) on qualifying days (X) was analyzed. This study uses a limit of 0.1 mm/day to classify wet and dry days and 1 mm precipitation as the

interval to further classify the precipitation class limits. The numbers of days will be counted for each class. Furthermore, the precipitation amount for each class and the cumulative total precipitation will be calculated. The exponential curve X versus Y is derived:

$$Y = aX\ exp(bX) \tag{5}$$

where a and b are constants estimated by the least-squares method. According to Martin-Vide (2004), one approach to adapt the above curve from the equation is through the curve:

$$Y = X \exp\left[-b(100 - X)^c\right] \tag{6}$$

where b and c are regression coefficient estimated using the least-squares method with observed precipitation data (Ananthakrishnan and Soman, 1989).

Both equations generate a polygonal line called the concentration curve, or Lorenz curve (Martin, 2004). The area S circled by the bisector of the quadrant, and the polygonal line provides a measure of the concentration. Gini concentration defined by $2S/10000$ is used to quantify the concentration. The area S for Equations (1) and (2) is the difference between 5000 and the definite integral of the Lorenze curve and can be written as:

$$S = 5000 - \int_0^{100} ax \exp(bx)\, dx \tag{7}$$

$$S = 5000 - \int_0^{100} x \exp[-b(100 - X)^c] dx \tag{8}$$

Then, the PCI can be expressed by

$$PCI = \frac{S}{5000} \tag{9}$$

The PCI index reveals the cumulative precipitation amount contributed by the cumulative number of precipitation days. A higher precipitation concentration is represented by greater percentages of the total annual precipitation on the rainy days.

In conclusion, the research methodology is depicted schematically in Figure 3.2. The LULC maps in 1992 and 2015 collected from European Space Agency are used to generate a transition matrix by Land Change Modeler. Furthermore, LULC is predicted for the future scenario (2040) based on the transition potential of various land use categories. Future climate change results under RCP 4.5 derived from GCMs are downscaled and interpolated to serve as climate input to the SWAT model. The M-K test is used identify the trends in historical and future meteorological variables. Three precipitation heterogeneity indices are also introduced to examine the climatic variability. After scenario design, streamflow and sediment yields under four scenarios

defined above can be simulated via SWAT. Finally, the hydrological responses under synergistic climate and LULC changes are examined.

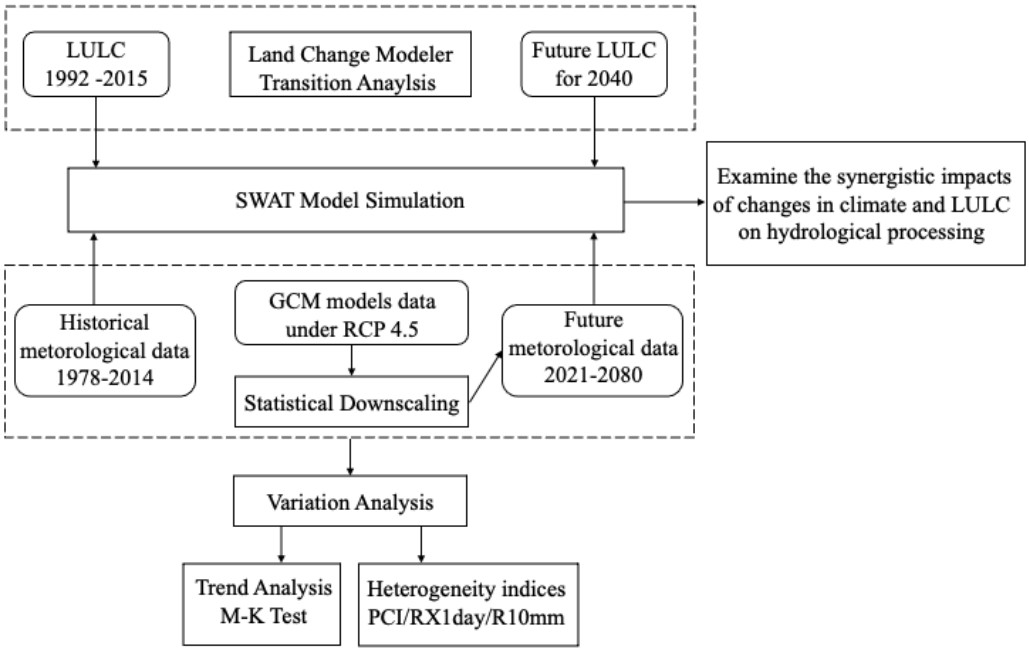

Figure 3.2 Schematic diagram of the research methodology.

CHAPTER 4: Results and Discussion

4.1 Climate Projection and Analysis

The historical climatic variables recorded for 33 selected weather stations within or close to the upper LRB are collected from 1978 to 2014. The future climate weather variables derived from CMIP5 are interpolated into 33 weather stations from 2021 to 2080. In this section, the historical and predicted time series of annual precipitation, maximum and minimum temperature (Figure 4.1 to Figure 4.6) are analyzed based on the M-K test.

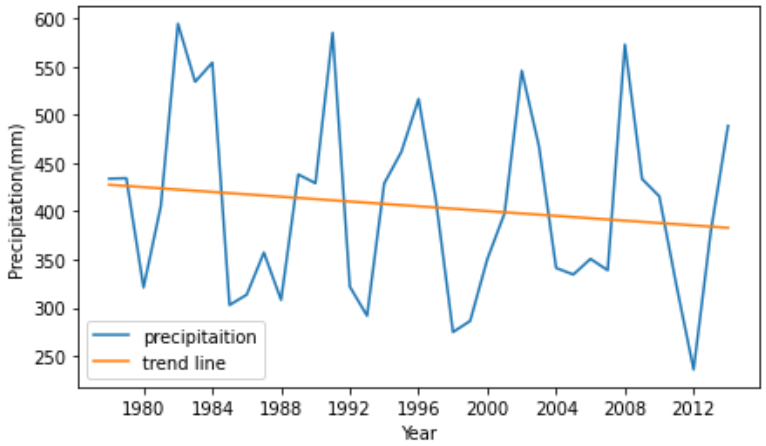

Figure 4.1 Time series of historical annual precipitation (mm) in the upper LRB.

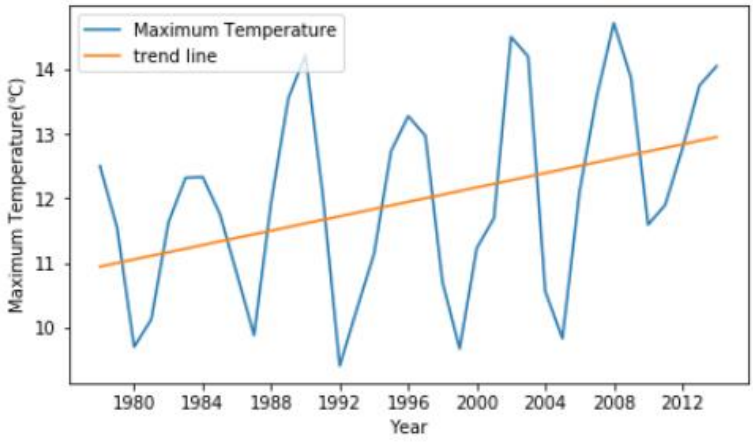

Figure 4.2 Time series of historical annual maximum temperature (°C) in the upper LRB.

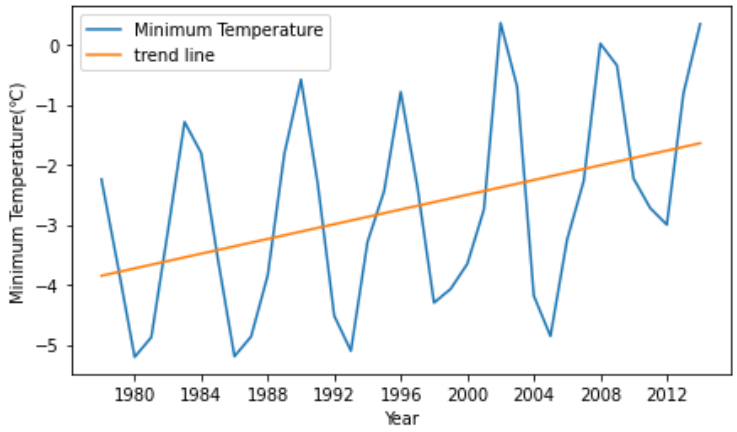

Figure 4.3 Time series of historical annual minimum temperature (℃) in the upper LRB.

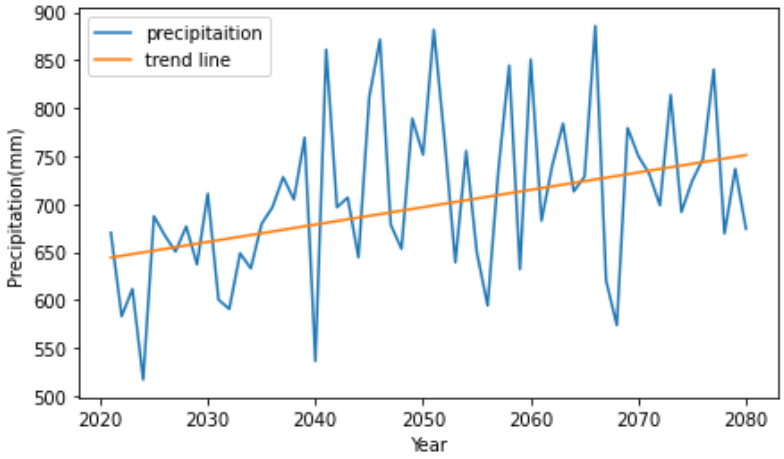

Figure 4.4 Time series of predicted annual precipitation (mm) in the upper LRB.

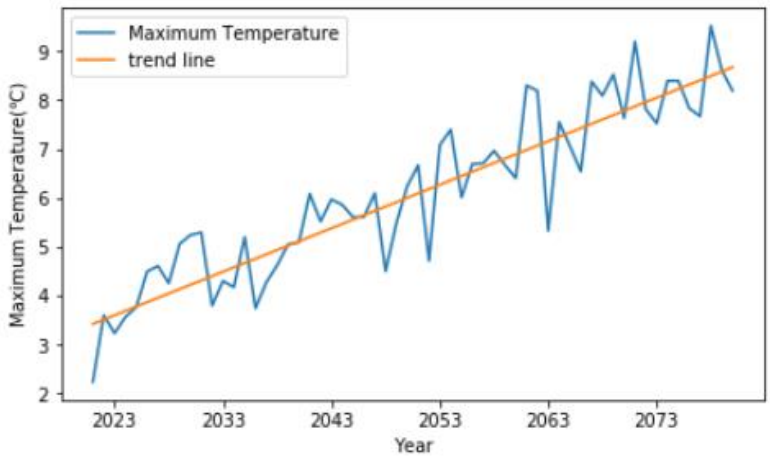

Figure 4.5 Time series of predicted annual maximum temperature (℃) in the upper LRB.

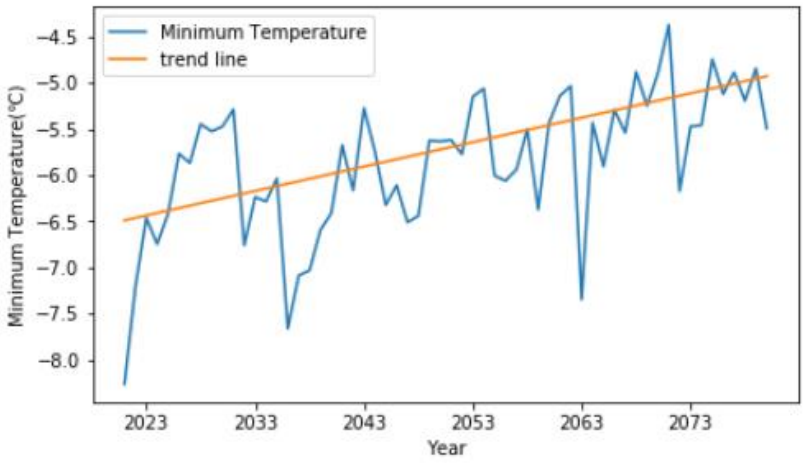

Figure 4.6 Time series of predicted annual minimum temperature (℃) in the upper LRB.

The time series of annual average precipitation, maximum and minimum temperature are statistically analyzed for both historical and future periods (Table 4.1). The results of M-K tests can be used to determine the significance of trends in climatic variables within a river basin. A positive Z value indicates that the time series has an increasing trend. The standard normal statistics $|Z| \geq 1.96$ confirms that the trend of the time series is statistically significant. If p-value is less than the significance level $\alpha = 0.05$, the null hypothesis is rejected, and the thus trend is significant.

During the period 1978 - 2014, annual maximum temperature and minimum temperature show significant positive trends. The results imply that the annual maximum and minimum temperature increased by 0.056℃ per year and 0.061℃ per year, respectively. However, there is a non-significant downward trend in the time series of precipitation in the historical period.

According to the M-K results for the future period from 2021 to 2080, the basin shows an obvious rising trend, which is greater than the trend observed in the historical period for all climatic variables. The future annual maximum and minimum temperature show significant positive trends of 0.089℃ per year and 0.026℃ per year, respectively. The future warming is roughly four times faster than the global average warming rate. In addition, the trend of maximum temperature will be more remarkable than that of minimum temperature, which indicates a higher extreme climate event frequency in the future. Furthermore, an upward trend for rainfall is statistically showed at a rate of 1.81 mm per year. Overall, the upper LRB becomes warmer and wetter at a faster rate higher than other regions in the world.

Table 4.1: M-K test statistics for annual maximum and minimum temperature, precipitation.

Time series	First year	Last Year	Test Z	p	slope	h	Trend
Precipitation (mm)	1978	2014	-0.719	0.471932	-1.2389	FALSE	No Trend
Max. Temperature (°C)	1978	2014	2.158	0.030927	0.05565	TRUE	Increase
Min. Temperature (°C)	1978	2014	2.2888	0.022091	0.06135	TRUE	Increase
Time series	**First year**	**Last Year**	**Test Z**	**p**	**slope**	**h**	**Trend**
Precipitation (mm)	2021	2080	2.94022	0.003280	1.81123	TRUE	Increase
Max. Temperature (°C)	2021	2080	8.48902	0.0	0.08893	TRUE	Increase
Min. Temperature (°C)	2021	2080	5.23627	0.001638	0.02645	TRUE	Increase

4.2 Precipitation Variability Analysis

Climate change affects the precipitation concentration, volume, and intensity, which further alters the hydrological responses within a river basin. In this study, the variability of precipitation is statistically analyzed based on three indices.

Precipitation Concentration Indices (PCI) is calculated to detect precipitation concentrations and their associated patterns. A higher PCI value indicates that the precipitation is more concentrated during the rainy days. The time series of annual PCI is analyzed by the M-K test for the whole period. P-value of the significance test and Z value is calculated to be 0.00719 and -2.6185, respectively. As a result, there is a significant decreasing trend of PCI, which implies that distribution of intra-annual precipitation within the basin will be more uniform in the future.

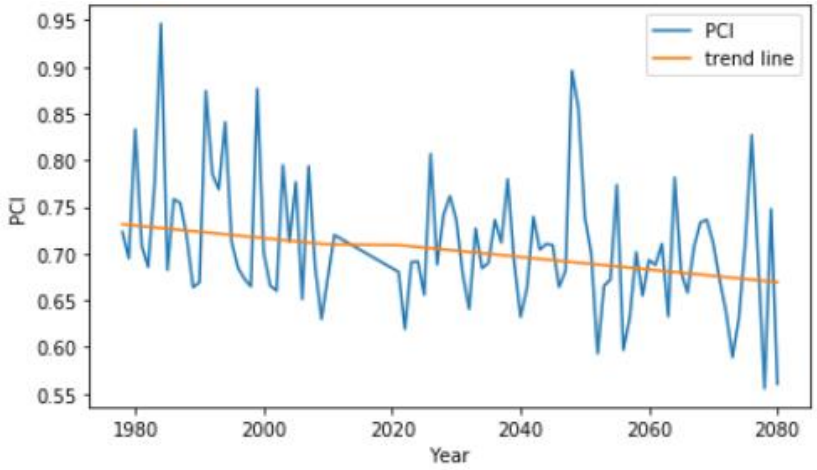

Figure 4.7 Time series of PCI in the upper LRB during the whole period.

Extreme precipitation events are also investigated using two additional indices: maximum 1-day precipitation (RX1day) and the number of heavy precipitation days (R10mm) (Song et al., 2015). RX1day describes the annual maximum 1-day precipitation. R10mm represents the number of days per year characterized by heavy (≥10 mm/d, R10mm). RX1day and R10mm are used to temporally analyze the extreme precipitation events on an annual scale throughout time.

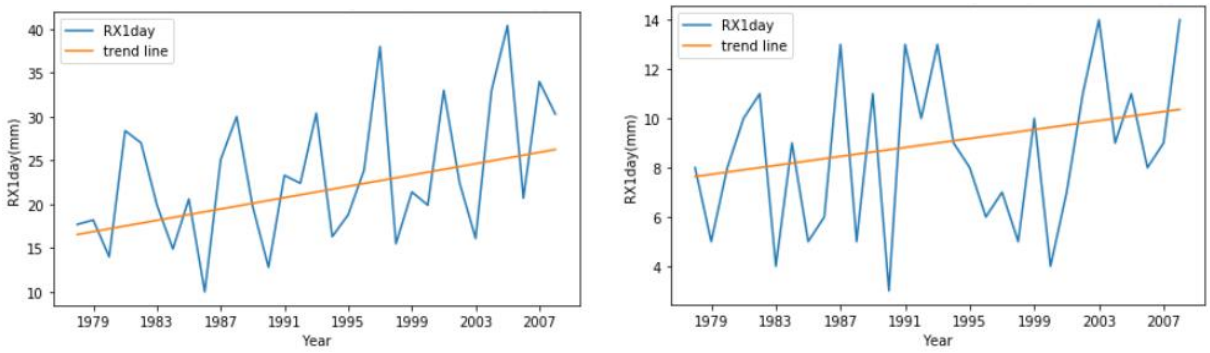

Figure 4.8 Time series of historical and predicted maximum 1-day precipitation (mm).

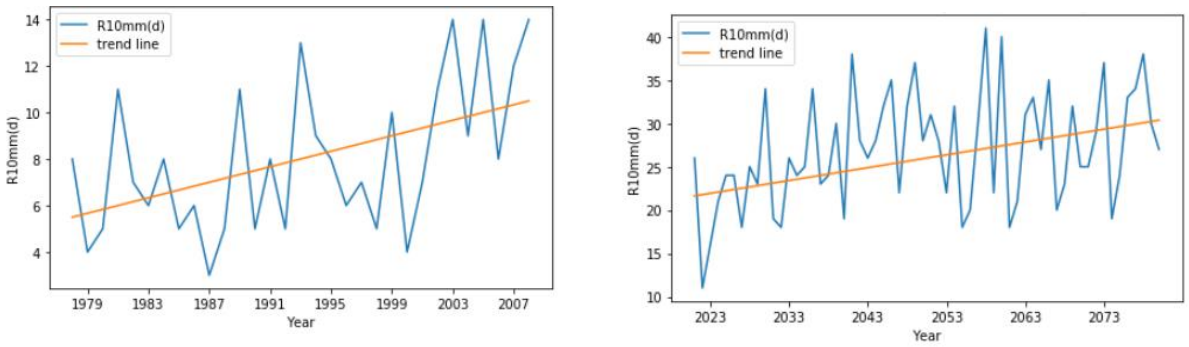

Figure 4.9 Time series of historical and future number of heavy precipitation days (d).

The variation trends of the time series of RX1day and R10mm are examined by the M-K test and shown graphically in Figure 4.8 and Figure 4.9. From the M-K results, |Z| values greater than 2.5 are calculated in the trend analysis of two indices, indicating prominent rising trends at a high confidence level. The results reveal that both RX1day and R10mm increase considerably during the whole period.

Table 4.2: Time series of historical and predicted number of heavy precipitation days.

Time series	First year	Last Year	Test Z	p	slope	h	Trend
PCI	1978	2080	-2.6185	0.008830	-0.0061	TRUE	Decrease
RX1day (mm)	1978	2014	2.2615	0.023728	0.3230	TRUE	Increase
	2021	2080	3.6866	0.000227	0.0885	TRUE	Increase
R10mm (day)	1978	2014	2.5896	0.009607	0.1666	TRUE	Increase
	2021	2080	2.6256	0.008647	0.1481	TRUE	Increase

In summary, the Precipitation Concentration Index shows a slightly downward trend, which means the intra-annual precipitation will be more evenly distributed in the future. Therefore, the increase in precipitation is accompanied by a decrease in the concentration index. RX1day and R10mm are introduced to directly assess the variation of extreme precipitation events in the future. According to the M-K test results, there is an increasing trend of the number of days when daily precipitation greater than 10 mm and the maximum daily precipitation in the future. As a result, higher frequency of extreme precipitation may accelerate the soil erosion in the study area in the future.

4.3 LULC Change Projection and Analysis

In the upper LRB, land use and land cover has experienced considerable transformations in recent years. In this study, three LULC maps are required to represent land use in three different scenarios: historical (1992), current (2015) and future (2040). Using the historical rates of change and the transition potential model, Land Change Modeler predicts the land use map for the year 2040 (Figure 4.10).

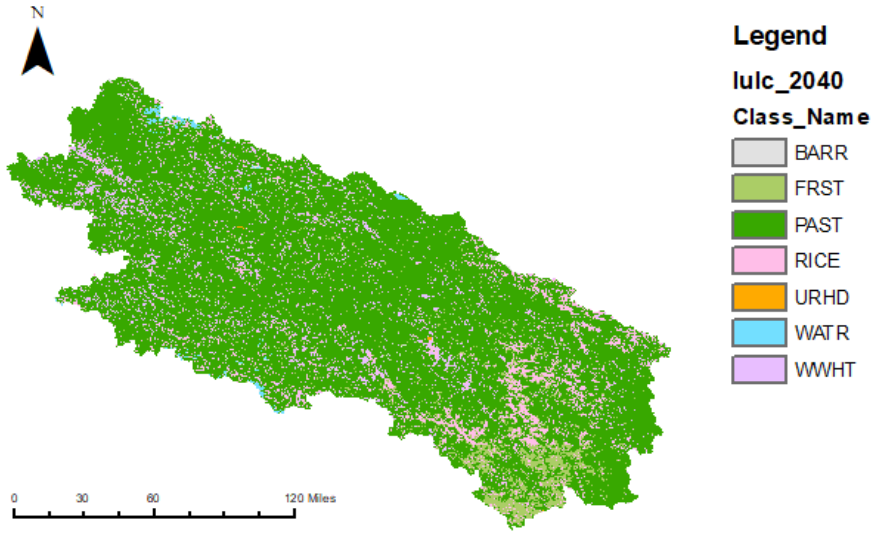

Figure 4.10 Predicted LULC map for the year 2040 in the upper LRB.

The land use change map (Figure 4.11) shows the spatial distribution of land use transition across the river basin from 1992 to 2015. In the upper LRB, the southern part has a higher potential of transition relative to the northern part.

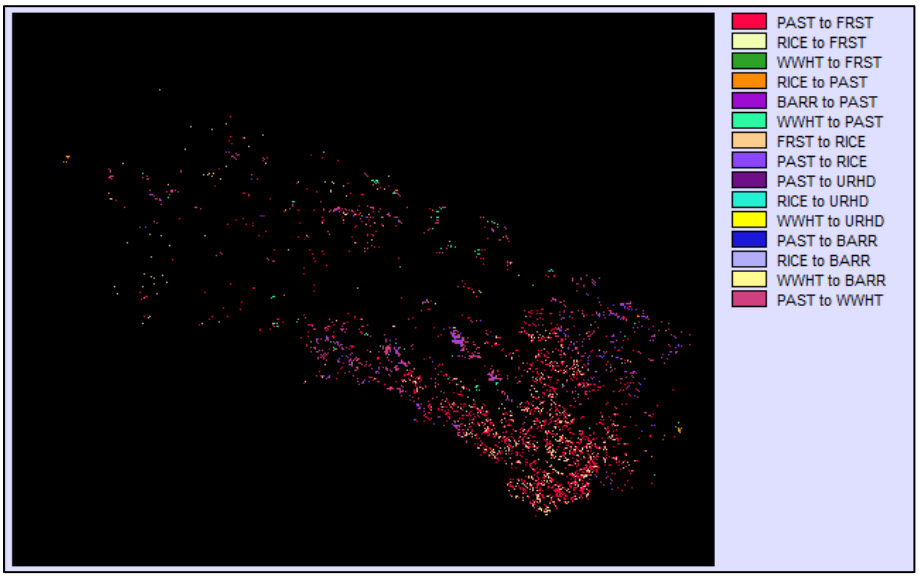

Figure 4.11 LULC change map from 1992 to 2015 in the upper LRB.

The transition probability matrix (Table 4.3) indicates the probability of changing from a given type to a target type. From the matrix results, the primary transitions are from forest to rice, pasture to forest, and pasture to cropland. It was found that human influence is rising in the upper LRB through the transformation from herding to cultivation, which results in an increase in cropland area.

Table 4.4 summarizes the changes in the composition of LULC in the upper LRB. Comparing the land use in 1992 and 2040, forest, rice and wheat acreage increases by 50.29%, 78.25% and 40.35%, respectively. Cropland areas expand the most among all the LULC classifications, while pasture lands continue to decline. Cultivated lands expand by 8906.26 km^2 per year, while the pasture areas decrease by 5.03% from 1992 to 2040. Simultaneously, with the development of the social economy, the urban area increased to 111km^2. However, the urban areas still account for a small proportion of the total area in the basin.

Table 4.3: Land use change map from 1992 to 2015 and transition matrix.

	FRST	PAST	RICE	URHD	BARR	WATR	WWHT
FRST	0.7086	0.0000	0.2914	0.0000	0.0000	0.0000	0.0000
PAST	0.0276	0.9554	0.0034	0.0001	0.0000	0.0000	0.0135
RICE	0.0000	0.0114	0.9882	0.0004	0.0000	0.0000	0.0000
URHD	0.1667	0.1667	0.1667	0.0000	0.1667	0.1667	0.1667
BARR	0.0000	0.0005	0.0000	0.0000	0.9995	0.0000	0.0000
WATR	0.0000	0.0000	0.0000	0.0000	0.0000	1.0000	0.0000
WWHT	0.0000	0.0258	0.0001	0.0007	0.0000	0.0000	0.9734

Table 4.4: Land use composition in the upper LRB.

Type	**1992**	**2015**	**2040**	**% Change**
FRST	25534	33044	38374	50.29%
PAST	575476	552855	546541	-5.03%
RICE	24998	33653	44560	78.25%
URHD	0	86	111	-
BARR	4271	4281	4237	-0.80%
WATR	2973	2973	2923	-1.68%

4.4 Correlation of Land Cover with Climate Factors

Changes in climate and LULC can result in the alterations of watershed hydrology. However, the synergy between land use and climate change may exacerbate the impacts of climate variables. Therefore, the impact of climate variables on vegetation growth is meaningful to evaluate in the alpine pastoral regions.

Normalized Difference Vegetation Index (NDVI) is selected as the vegetation index to represent the vegetation cover quality in this study. A regression model between NDVI and climate change variables is set up to exploit the climate change impacts on land cover. Moderate Resolution Imaging Spectroradiometer (MODIS) Vegetation Indices (MYD13Q1) V6 data during the plant growth season (May to October) from 2002 to 2020 are collected.

The average NDVI value during the plant growth season for the past 18 years is calculated. The positive NDVI represents that there is vegetation present, and a higher value indicates that the vegetation is in better condition. The results show a significant rising trend of NDVI in the study area. In the past 20 years, the basin averaged NDVI during the plant growth season has increased by almost 9%.

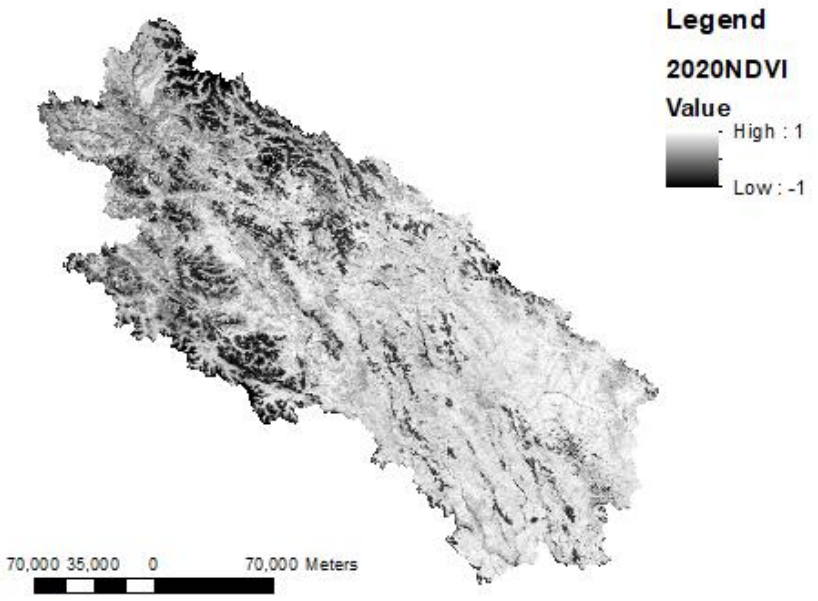

Figure 4.12 Average NDVI spatial distribution during the plant growth season in 2020.

The correlation of vegetation with precipitation and temperature was analyzed at the basin scale:

$$RP = \frac{\sum(NDVI_i - \overline{NDVI}) * (P_i - \bar{P})}{\sqrt{\sum(NDVI_i - \overline{NDVI})^2 * \sum(P_i - \bar{P})^2}} \quad (10)$$

$$RT = \frac{\sum(NDVI_i - \overline{NDVI}) * (T_i - \bar{T})}{\sqrt{\sum(NDVI_i - \overline{NDVI})^2 * \sum(T_i - \bar{T})^2}} \quad (11)$$

RP and RT are the correlation coefficient of vegetation with precipitation and temperature in the basin scale, respectively.

As a result,

$$RP = 0.537, RT = 0.614$$

Based on correlation analysis, comparing with the correlation coefficients of vegetation with precipitation and temperature, the dominant variable for vegetation cover change can be identified. Correlation analysis reveals that the increase in NDVI might be attributed to more favorable climatic conditions, as vegetation positively correlated with annual temperature and precipitation. In addition, RT is greater than RP, indicating that temperature has stronger effects on plant production in the alpine meadows. As a conclusion, the tight relationship between vegetation and climatic factors demonstrates the need of considering the synergistic impacts of environmental changes.

4.5 SWAT Calibration and Validation

Due to the scarcity of hydrological stations in the upper Lancang River Basin, a SWAT model for the whole Lancang River Basin developed by Xu et al. (2020) is utilized to assist in determining the parameters for the upper LRB SWAT model. Monthly flow and sediment load observations were obtained at three hydrological stations. The SWAT model was calibrated for streamflow and sediment using an automated calibration model (Soil and Water Assessment Tool Calibration and Uncertainty Procedure, SWAT-CUP). The most influential parameters for the hydrological model were chosen in the calibration procedure based on preliminary sensitivity analysis and previous studies (Luo et al., 2008; Li et al., 2010; Zheng and Han, 2016). Five sensitive parameters were considered when calibrating streamflow. The observed data at Jiajiu and Jiuzhou Stations were split for calibration (1982–2002) and validation (2003–2008) purpose. The observed data from the Yunjinghong Station were split for calibration (1982–2002) and validation (2003–2008) due to the lack of data. Seven sensitive parameters were considered when calibrating sediment yields. The observed data were split for calibration (1980–1984) and validation (1985-1986).

Calibration and validation results for the Lancang River Basin are showed in Figure 4.15, based on the study of Xu et al. (2020). For the calibration and validation periods, the Nash–Sutcliffe efficiency coefficient, NS (Nash and Sutcliffe, 1976), for streamflow and sediment loads is between 0.87 and 0.94. The NS statistic is used to assess the fit between simulated and observed

data. Additionally, higher values of R2 (0.93-0.96) obtained during the calibration and validation period show a strong correlation between observed and simulated streamflow and sediment loads. In general, the SWAT model performs well in the Lancang River Basin for the two target variables.

In the upper Lancang River Basin, parameters related to streamflow and sediment are considered and 16 parameters are identified as the most sensitive parameters for calibration. Table 4.5 shows the original range and calibrated values. The calibrated values for the study site are derived from the previous studies and initial range, which varying for different subbasins and reaches, as well as land cover and soil type. According to the table, the most sensitive parameter in the upper LRB is CN2 (moisture condition II curve number). Based on the calibrated values of parameters, the SWAT model simulates the monthly streamflow and monthly sediment loads in the upper Lancang River Basin (Figure 4.13 and 4.14).

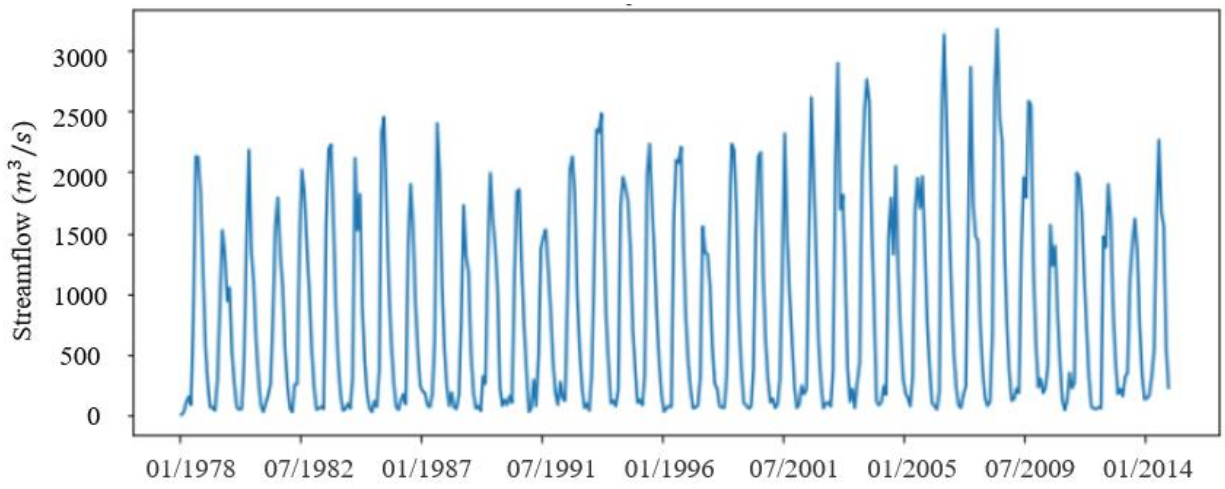

Figure 4.13 Simulated monthly streamflow (m^3/s) at the outlet.

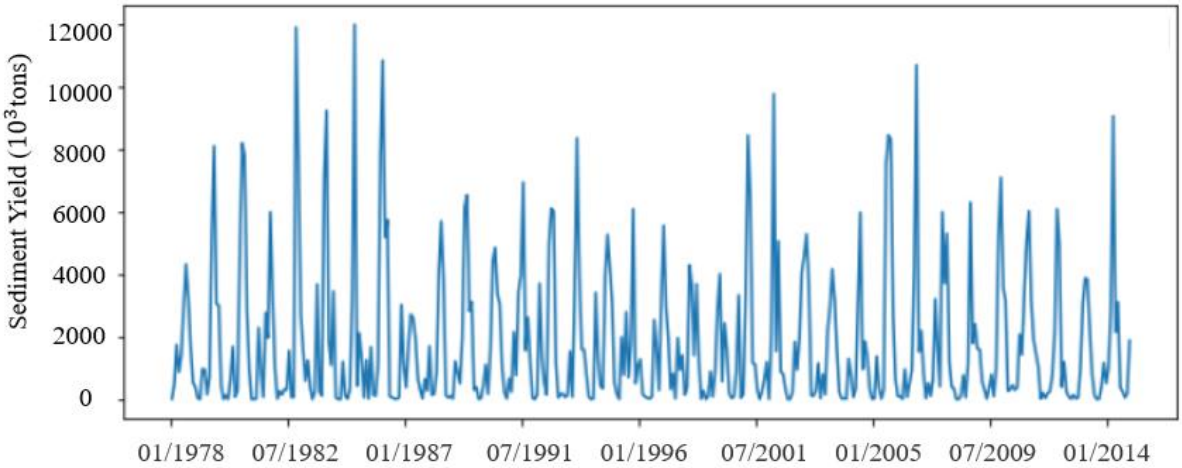

Figure 4.14 Simulated monthly sediment yield (10^3 tons) at the outlet.

Table 4.5: Ranges and calibrated values of the major SWAT parameters.

Target variables	Parameter	Description	Initial range	Calibrated values
Streamflow	CN2	Initial SCS runoff curve number for moisture condition II	35–98	$53.2-67.4^{b}$
	ALPHA_BF	Baseflow alpha factor (days)	0–1	$0-0.04^{a}$
	GWQMN	Threshold depth of water in the shallow aquifer required for return flow to occur (mm).	0–500	$15-357^{a}$
	ESCO	Soil evaporation compensation factor	0–1	$0.1-1^{a}$
	SURLAG	Surface runoff lag time	0.05–0.10	0.05
	OV_N	Manning's "n" value for overland flow	0.01–1	$0.12-0.23^{b}$
	SOL_AWC	Available water capacity of the soil layer	0–1	$0.05-0.53^{b}$
	CH_K2	Effective hydraulic conductivity in main channel alluvium.	0.01–50	$15.8-23.9^{a}$
	CH_N1	Manning's "n" value for the tributary channels	0.01–0.3	$0.05-0.10^{a}$
	ALPHA_BNK	Baseflow alpha factor for bank storage	0–1	$0.05-0.94^{a}$
	GW_REVAP	Groundwater delay (days)	0.02–0.20	$0.05-0.16^{a}$
Sediments	USLE_P	USLE equation support practice factor	0–1	$0.27-0.89^{a}$
	SPEXP	Exponent parameter for calculating sediment retrained in channel sediment routing	1–1.5	1.38
	SPCON	Linear parameter for calculating the maximum amount of sediment that can be retrained during channel sediment routing	0.0001–0.01	0.00018
	PRF_BSN	Peak rate adjust factor for sediment routing in the main channel	0–2	2
	USLE_C	Min value of USLE C factor applicable to the land cover/plant	0.001–0.5	$0.09-0.43^{b}$

^{a} Varying for different sub-basins or reaches; ^{b} Varying for different land covers or soil types.

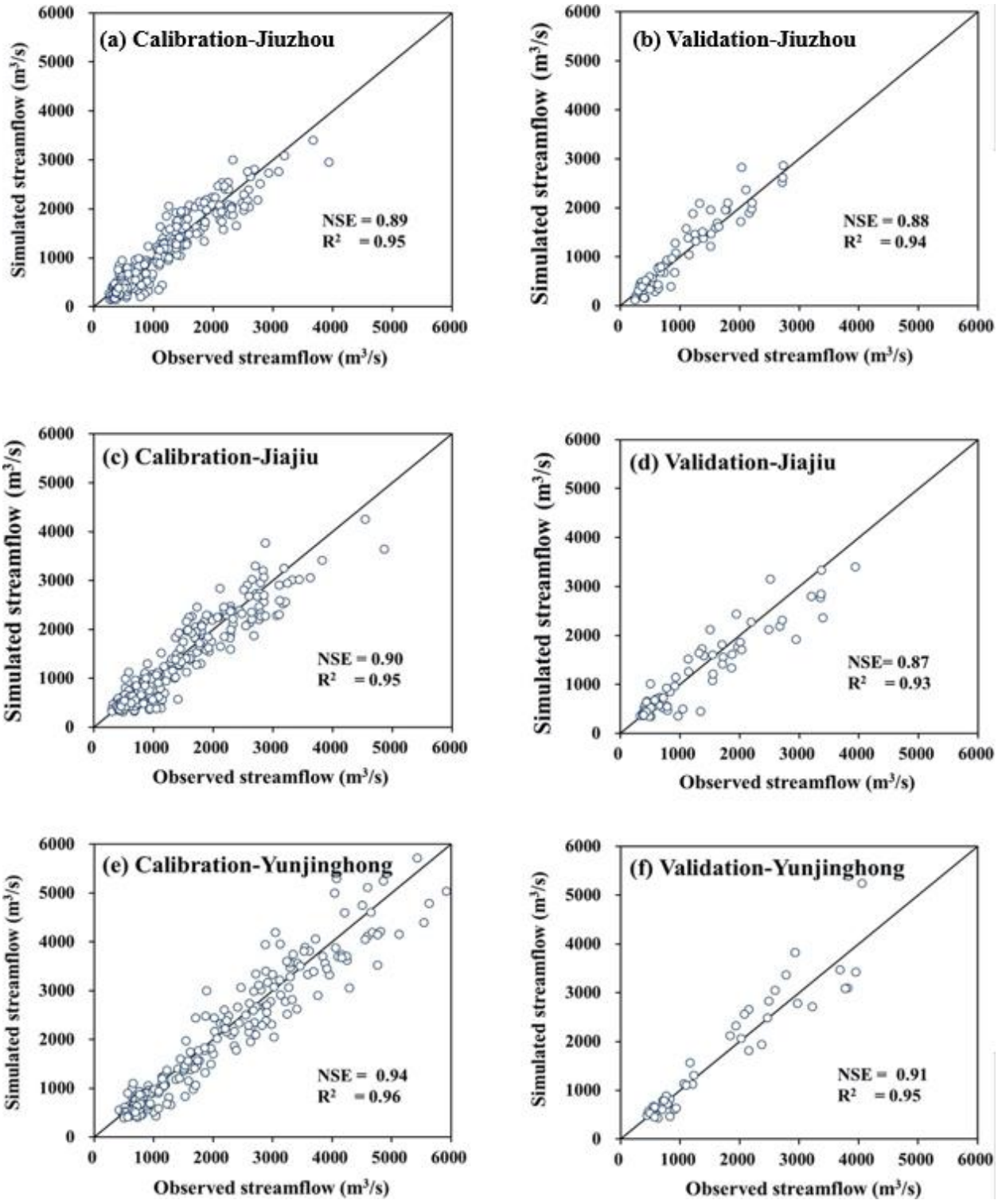

Figure 4.15 Observed and simulated monthly streamflow at Jiuzhou, Jiajiu and Yunjinghong Stations. (a), (c) and (e) are for the calibration period, and (b), (d) and (f) are for the validation period. The solid line is the 45-degree line for comparison.

4.6 Spatiotemporal Distribution of Hydrological Processing

4.6.1 Temporal Distribution of Sediment Yield

To identify the effects of environmental factors on the temporal variation of sediment yield, four comprised of various climatic and land use data are separately fed into the SWAT model. From Figure 4.16 to Figure 4.21, the time series of simulated annual/monthly accumulated sediment yield and the spatial distribution of simulated annual/monthly accumulated sediment yield are presented.

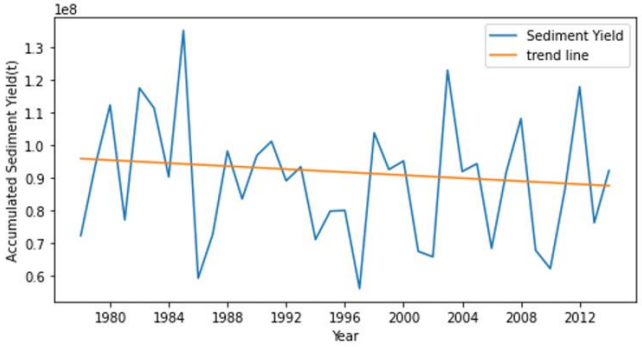

Figure 4.16 Simulated Annual Accumulated Sediment Yield under Scenario 1.

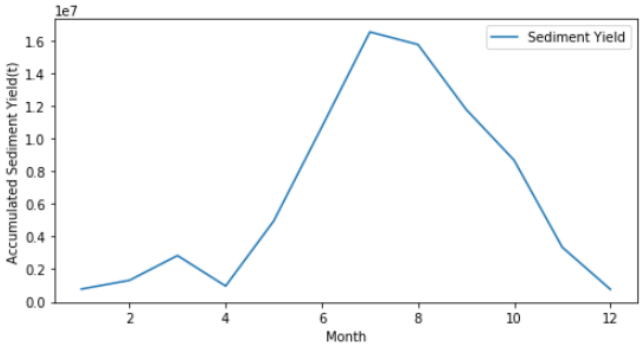

Figure 4.17 Simulated Monthly Accumulated Sediment Yield under Scenario 1.

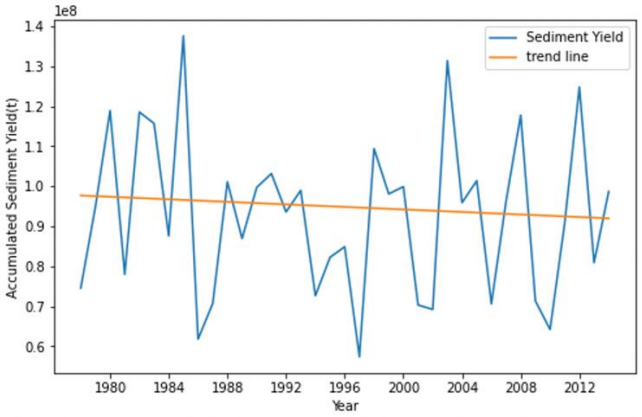

Figure 4.18 Simulated Annual Accumulated Sediment Yield under Scenario 2.

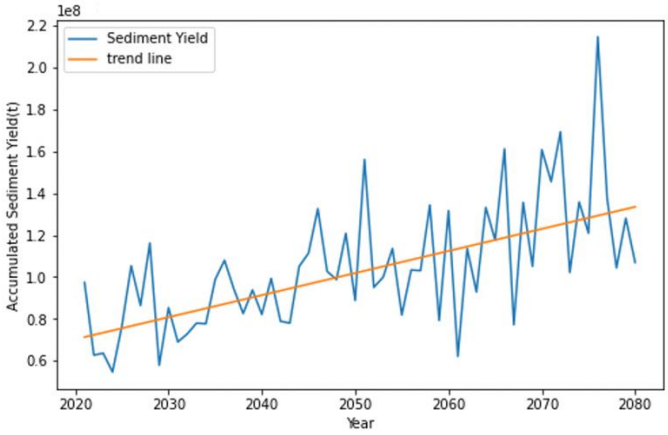

Figure 4.19 Simulated Annual Accumulated Sediment Yield under Scenario 3.

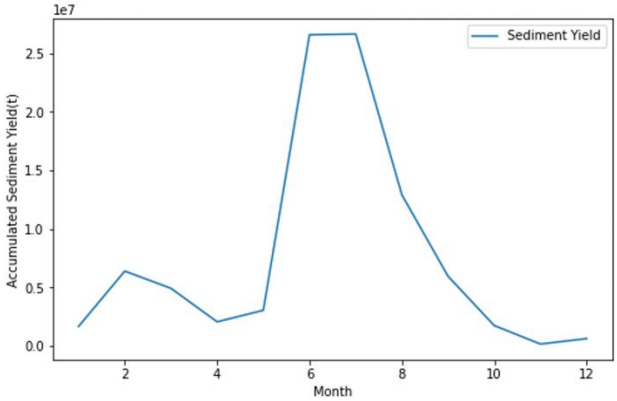

Figure 4.20 Simulated Monthly Accumulated Sediment Yield under Scenario 3.

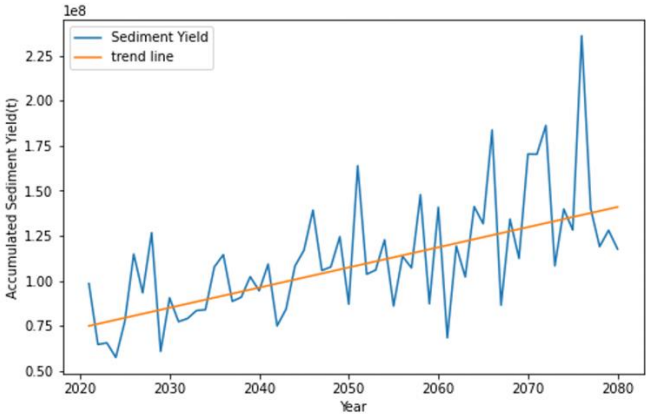

Figure 4.21 Simulated Annual Accumulated Sediment Yield under Scenario 4.

Table 4.7 compares the results of all scenarios and illustrates the changes in average annual sediment yield under various scenarios. The greater value of sediment yield represents the significant soil erosion in the absence of soil conservation intervention. Sediment losses form the

landscape are determined by a variety of causes. By comparing simulation results from four scenarios, the individual and synergistic effects of two environmental factors on hydrological processing over time may be quantified. In comparison to scenario 1, the annual average accumulated sediment yield increases by 5.0%, 17.9% and 25.9% for scenarios 2, 3, and 4, respectively.

Table 4.6: Comparison of scenario results to show % change in annual sediment yield.

Scenario	Sediment yield (10^3 tons)	% Change
1	89108.745	-
2	93545.099	4.978%
3	105057.511	17.898%
4	112213.850	25.929%

In scenario 1, the M-K test indicates that there is no discernible trend detected in the time series of annual accumulated sediment yield (Figure 4-16). However, the sediment yield variation pattern is clearly identified at the monthly scale (Figure 4-17). The sediment yield in wet season accounts for the vast majority part of precipitation in the year. Monthly accumulated sediment yields reach a maximum of 16.53 million tons.

In scenario 2, the historical map is superseded by the present land use map. The simulation results indicate that sediment yields increase with land use transformation (Figure 4-18). Relative to scenario 1, the annual sediment yield increases by 5.0 % in the historical period. The expansion of agriculture and urban areas at the expense of pastureland is the primary reason for the negative effects on sediment production. According to Table 4.3, the primary land use change between 1992 and 2015 was the conversion of some pastureland to crops. Soil erosion is accelerated on land when erosive rain falls on deforested and agricultural landscapes. Meanwhile, urbanization might result in the expansion of pervious areas and a decrease in vegetation coverage. As a result, cropland depicts the highest rate of erosion among the primary land cover types, whereas forest usually exhibit lower rates of erosion than pasture.

Climate change impacts may be assessed using simulations under climate-change-only scenarios. In scenario 3, predicted daily precipitation, minimum and maximum temperatures, and precipitation data are used for SWAT simulation. The M-K test demonstrates that in the future scenario, annual accumulated sediment yield grows substantially. According to the pattern of

monthly sediment yield variation, most of the sediment yield occurs during the rainy season. The annual average sediment yield increases by 12.4% comparing with scenario 2. The findings show that climatic variables are the primary determinants of sediment yield variation.

To further investigate the synergistic effects of environmental factors, scenarios including concurrent changes in climate and land use are explored. Scenario 4 represents a future scenario when cropland occupies a larger proportion of the basin area. According to the modeling findings (Figure 4-21), the LULC modification is anticipated to result in a substantial increase in sediment yield. In comparison to scenario 3, land use conversion results in an increase of 6.8% of the annual sediment yield under future climate condition, which is greater than the results under historical climate conditions.

4.6.2 Spatial Distribution of Sediment Yield

Apart from the temporal distribution, the spatial distribution of sediment yield is also simulated. Figure 4.22 depicts the simulated spatial distribution of annual average sediment yield at the subbasin scale Barren area and farmland are the major land use categories in the southwestern and central subbasins with the highest sediment yield. The area in the southern portion of the basin with the greatest potential for transition from pasture to cropland has a greater sediment yield due to climate change and changes in land use and cover.

The simulation results show that climate and LULC changes have occurred at both basin and sub-basin levels. Furthermore, the impacts of land use change on the water balance vary for each sub-basin. Some sub-basins show a distinct pattern of change in terms of hydrologic components. Without soil conservation measures, subbasins transitioning from pasture to agriculture will continue to suffer from soil erosion in the future.

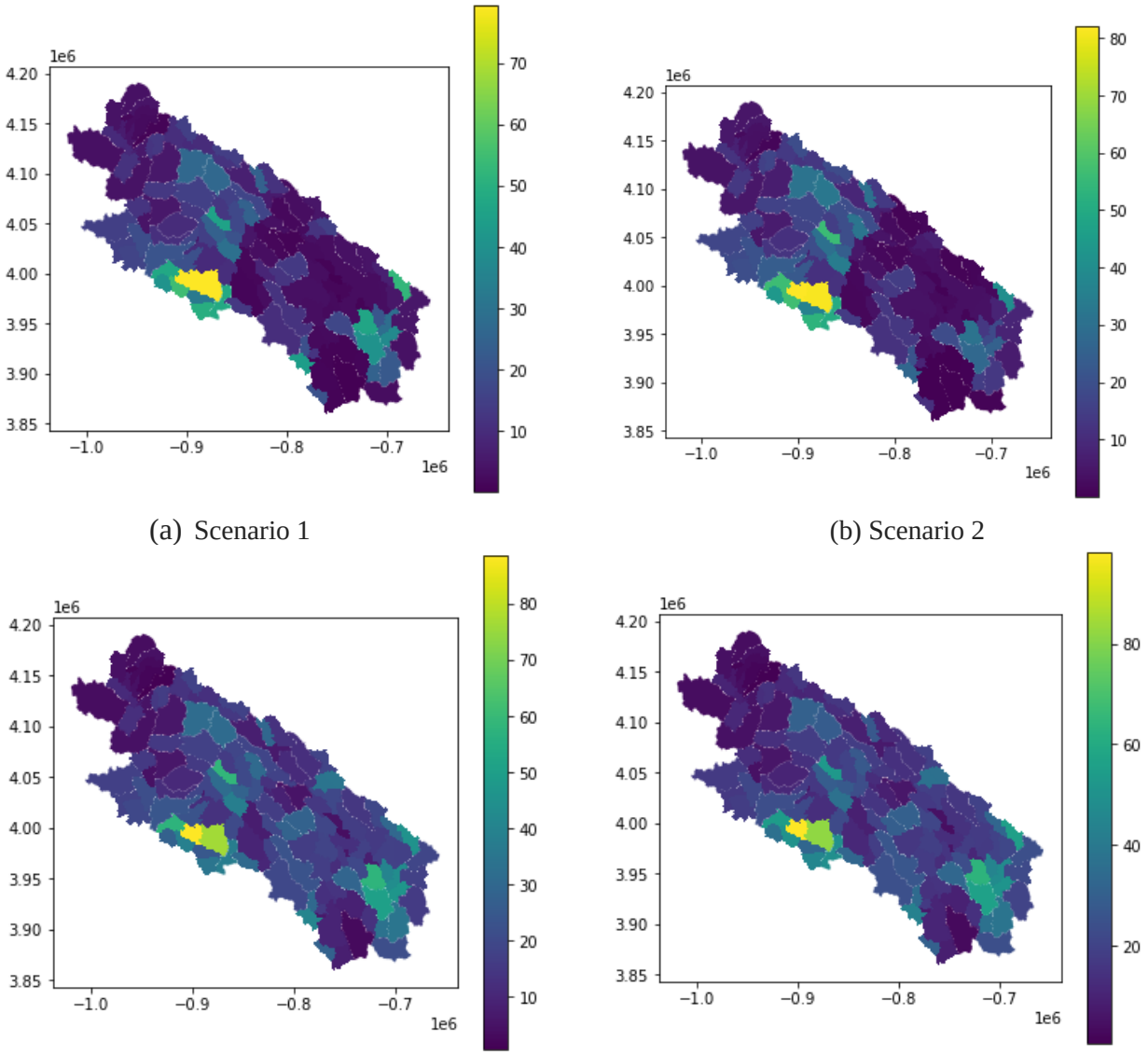

(a) Scenario 1 (b) Scenario 2

(c) Scenario 3 (d) Scenario 4

Figure 4.22 Spatial Distribution of Accumulated Sediment Yield under 4 Scenarios.

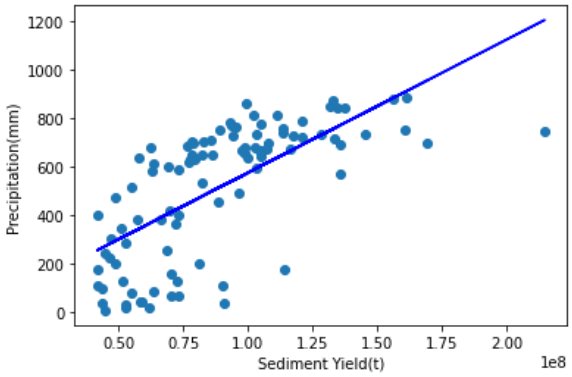

Figure 4.23 Linear Regression between Sediment Yield (t) and Precipitation (mm).

Additionally, similar patterns and variations are observed in sediment yield and precipitation in the upper LRB. The result in Figure 4.23 shows that precipitation has a positively high correlation with sediment yield, with the coefficient of determination being 0.6794. The results demonstrate that even minor reduction in seasonal and annual precipitation may have large effects on sediment yield in the upper LRB.

CHAPTER 5: Conclusion

In this study, a semi-distributed hydrological model (SWAT) is set up for the upper Lancang River Basin, a basin in an alpine pastoral region; four scenarios combining climate change and land use conditions are simulated to quantify the hydrologic response to the environmental changes. Statistical tests are conducted to identify trends in both historical and future period.

In the historical period of 1978 - 2014, the temperature showed a remarkable upward trend, whereas the precipitation displayed a non-significant downward trend. The wet season last from May to October, which accounts for more than 80% of the annual precipitation. In the future period, it is found that the climate in the basin will likely to be warmer and wetter. More specifically, as the trend analysis result shows, the temperature can have a significant rising trend in the upper LRB, with a much higher rate than the global average warming rate; the rising trend predicted with extreme precipitation events is more obvious than that with the historical period.

The vegetation cover will change driven by climate change and land use transition. As predicted by the Land Change Modeler, the cultivation area will increase the most among all land use classes from now to 2040; meanwhile the pastureland will decline. In addition, the NDVI-climate regression analysis shows that NDVI has a strong positive correlation with temperature and precipitation, but temperature plays a major role in the spatiotemporal distribution of vegetation in the area.

As a result of the projected climate and land use change, strong effects on watershed hydrology are projected for both streamflow and sediment discharges in the area. In particular, the synergistic climate and LULC change may alter the hydrological regimes significantly by both time and space in the upper LRB. The simulation results under the four scenarios show that the runoff and sediment yield will experience a clear upward trend. Precipitation is the most sensitive factor affecting runoff and sediment yield in the river basin. Moreover, climate change will have substantial effects on land use by promoting the conversion from pasture to crop cultivation under a warmer and wetter climate, which will eventually accelerate the rate of soil erosion and sediment yield. Spatially, the predicted sediment yield in the southern part of the basin increases obviously due to higher transition potentials. Although the effect of climate change on sediment yield is higher than that of land use change, the synergistic effect of climate and land use change is stronger than the sum of their individual effects.

The results from the modeling exercises will provide supports for sustainable water resources management in the upper LRB, especially to deal with the challenges of climate change and associated land use and land cover change in the future. Conversions of land use patterns from forest or pastural land to crop land under conditions of climate change, which has been observed in the historical period, may strongly affect the natural system in the barely developed alpine pastoral regions, and should be avoided with certain regulations and incentives. Thus, measuring hydrologic responses to environmental changes allows the estimate the potential impacts on hydrologic processing under different land use planning and management scenarios, which may offer scientific supports for more appropriate land use management in the basin. Additionally, the spatial heterogeneity of hydrological responses enables the evaluation and identification of erosion-prone areas for the purpose of prioritizing sub-watershed conservation interventions and maximizing the utilization of scarce resources. The insights gained from this study may help decision-makers manage land and water resources holistically in alpine pastoral regions.

REFERENCES

Aawar, T. (1), & Khare, D. (2). (2020). Assessment of climate change impacts on streamflow through hydrological model using SWAT model: a case study of Afghanistan. Modeling Earth Systems and Environment, 6(3), 1427–1437. https://doi-org.proxy2.library.illinois.edu/10.1007/s40808-020-00759-0

Aboelnour, M., Gitau, M. W., & Engel, B. A. (2020). A comparison of streamflow and baseflow responses to land-use change and the variation in climate parameters using SWAT. Water, 12(1), 191.

Adamowski, K., & Bougadis, J. (2003). Detection of trends in annual extreme rainfall. Hydrological Processes, 17(18), 3547-3560.

Adhikari, S., Southworth, J., 2012. Simulating forest cover changes of Bannerghatta national park based on a CA-Markov model: a remote sensing approach. Remote Sens. 4:3215–3243. https://doi.org/10.3390/rs4103215.

Ahmad, I., Tang, D., Wang, T., Wang, M., & Wagan, B. (2015). Precipitation trends over time using Mann-Kendall and spearman's rho tests in swat river basin, Pakistan. Advances in Meteorology, 2015.

Amisigo, B. A., McCluskey, A., & Swanson, R. (2015). Modeling impact of climate change on water resources and agriculture demand in the Volta Basin and other basin systems in Ghana. Sustainability, 7(6), 6957-6975.

Ananthakrishnan, R., & Soman, M. K. (1989). Statistical distribution of daily rainfall and its association with the coefficient of variation of rainfall series. International Journal of Climatology, 9(5), 485-500.

Arnold, J. G., Moriasi, D. N., Gassman, P. W., Abbaspour, K. C., White, M. J., Srinivasan, R., ... & Jha, M. K. (2012). SWAT: Model use, calibration, and validation. Transactions of the ASABE, 55(4), 1491-1508.

Arnold, J. G., Srinivasan, R., Muttiah, R. S., & Williams, J. R. (1998). Large area hydrologic modeling and assessment part I: model development 1. JAWRA Journal of the American Water Resources Association, 34(1), 73-89.

Awotwi, A., Kumi, M., Jansson, P. E., Yeboah, F., & Nti, I. K. (2015a). Predicting hydrological response to climate change in the White Volta catchment, West Africa.

Awotwi, A., Yeboah, F., & Kumi, M. (2015b). Assessing the impact of land cover changes on water balance components of W hite V olta B asin in W est A frica. Water and Environment Journal, 29(2), 259-267.

Bonell, M., Purandara, B. K., Venkatesh, B., Krishnaswamy, J., & Acharya, H. A. K., Singh, UV,… Chappell, N.(2010). The impact of forest use and reforestation on soil hydraulic conductivity in the western Ghats of India: Implications for surface and sub-surface hydrology. Journal of Hydrology, 391(1), 47-62.

Briak, H., Moussadek, R., Aboumaria, K., & Mrabet, R. (2016). Assessing sediment yield in Kalaya gauged watershed (Northern Morocco) using GIS and SWAT model. International Soil and Water Conservation Research, 4(3), 177-185.Jayakumar, R., Chappell, N., 2010. The impact of forest use and reforestation on soil hydraulic conductivity in the Western Ghats of India: implications for surface and sub-surface hydrology.

Brown, A.E., Zhang, L., McMahon, T.A., Western, A.W., Vertessy, R.A., 2005. A review of paired catchment studies for determining changes in water yield resulting from alterations in vegetation. J. Hydrol. 310:28–61. https://doi.org/10.1016/j. jhydrol.2004.12.010.

Bunting, E. L., Fullman, T., Kiker, G., & Southworth, J. (2016). Utilization of the SAVANNA model to analyze future patterns of vegetation cover in Kruger National Park under changing climate. Ecological Modelling, 342, 147-160.

Chen, Q., Chen, H., Zhang, J., Hou, Y., Shen, M., Chen, J., & Xu, C. (2020). Impacts of climate change and LULC change on runoff in the Jinsha River Basin. Journal of Geographical Sciences, 30(1), 85-102.

Cuo, Y., Zhang, Y., Gao, Z., Hao, L. Cairang, 2013. The impacts of climate change and land cover/use transition on the hydrology in the upper Yellow River basin, China. J. Hydrol. 502 (2013):37–52. https://doi.org/10.1016/j.jhydrol.2013.08.003.

Dibaba, W. T. (1,2), Miegel, K. (1), & Demissie, T. A. (2). (2020). Watershed hydrological response to combined land use/land cover and climate change in highland ethiopia: Finchaa catchment. Water (Switzerland), 12(6). https://doi-org.proxy2.library.illinois.edu/10.3390/w12061801

Donner, L. J., Wyman, B. L., Hemler, R. S., Horowitz, L. W., Ming, Y., Zhao, M., ... & Zeng, F. (2011). The dynamical core, physical parameterizations, and basic simulation

characteristics of the atmospheric component AM3 of the GFDL global coupled model CM3. Journal of Climate, 24(13), 3484-3519.

Ezenwaji, E., Nzoiwu, C., & Chima, G. (2017). Analysis of precipitation concentration index (pci) for awka urban area, Nigeria. Hydrology: Current Research, 8(4), 1-6.

Finger, D., Pellicciotti, F., Konz, M., Rimkus, S., & Burlando, P. (2011). The value of glacier mass balance, satellite snow cover images, and hourly discharge for improving the performance of a physically based distributed hydrological model. Water Resources Research, 47(7).

Fyfe, J. C., Gillett, N. P., & Zwiers, F. W. (2013). Overestimated global warming over the past 20 years. Nature Climate Change, 3(9), 767-769.

Gassman, P. W., Sadeghi, A. M., & Srinivasan, R. (2014). Applications of the SWAT model special section: overview and insights. Journal of Environmental Quality, 43(1), 1-8.

Gebremicael, T. G., Mohamed, Y. A., Betrie, G. D., Van Der Zaag, P., & Teferi, E. (2013). Trend analysis of runoff and sediment fluxes in the Upper Blue Nile basin: A combined analysis of statistical tests, physically-based models and landuse maps. Journal of Hydrology, 482, 57-68.

Gosling, S. N., Taylor, R. G., Arnell, N. W., & Todd, M. C. (2011). A comparative analysis of projected impacts of climate change on river runoff from global and catchment-scale hydrological models. Hydrology and Earth System Sciences, 15(1), 279-294.

Griffies, S. M., Winton, M., Donner, L. J., Horowitz, L. W., Downes, S. M., Farneti, R., ... & Zadeh, N. (2011). The GFDL CM3 coupled climate model: characteristics of the ocean and sea ice simulations. Journal of Climate, 24(13), 3520-3544.

Hu, Q., Willson, G. D., Chen, X., & Akyuz, A. (2005). Effects of climate and landcover change on stream discharge in the Ozark Highlands, USA. Environmental Modeling & Assessment, 10(1), 9-19.

Jain, R. K., Jain, K., & Ali, S. R. (2017). Modeling urban land cover growth dynamics based on land change modeler (LCM) using remote sensing: a case study of Gurgaon, India. Advances in Computational Sciences and Technology, 10(10), 2947-2961.

Jayakrishnan, R. S. R. S., Srinivasan, R., Santhi, C., & Arnold, J. G. (2005). Advances in the application of the SWAT model for water resources management. Hydrological Processes: An International Journal, 19(3), 749-762.

Kafy, A. A., Shuvo, R. M., Naim, M. N. H., Sikdar, M. S., Chowdhury, R. R., Islam, M. A., ... & Kona, M. A. (2021). Remote sensing approach to simulate the land use/land cover and seasonal land surface temperature change using machine learning algorithms in a fastest-growing megacity of Bangladesh. Remote Sensing Applications: Society and Environment, 21, 100463.

Kamworapan, S., & Surussavadee, C. (2019). Evaluation of CMIP5 global climate models for simulating climatological temperature and precipitation for Southeast Asia. Advances in meteorology, 2019.

Kendall, M. G. (1948). Rank correlation methods.

Khare, D., Mondal, A., Kundu, S., & Mishra, P. K. (2017). Climate change impact on soil erosion in the Mandakini River Basin, North India. Applied Water Science, 7(5), 2373-2383.

Legesse, D., Vallet-Coulomb, C., & Gasse, F. (2003). Hydrological response of a catchment to climate and land use changes in Tropical Africa: case study South Central Ethiopia. Journal of hydrology, 275(1-2), 67-85.

Li, Z., Shao, Q., Xu, Z., & Cai, X. (2010). Analysis of parameter uncertainty in semi-distributed hydrological models using bootstrap method: A case study of SWAT model applied to Yingluoxia watershed in northwest China. Journal of Hydrology, 385(1-4), 76-83.

Luis, M. D., Gonzalez-Hidalgo, J. C., Brunetti, M., & Longares, L. A. (2011). Precipitation concentration changes in Spain 1946–2005. Natural Hazards and Earth System Sciences, 11(5), 1259-1265.

Luo, Y., Zhang, X., Liu, X., Ficklin, D., & Zhang, M. (2008). Dynamic modeling of organophosphate pesticide load in surface water in the northern San Joaquin Valley watershed of California. Environmental Pollution, 156(3), 1171-1181.

Mango, L.M., Melesse, A.M., McClain, M.E., Gann, D., Setegn, S.G., 2011. Land use and climate change impacts on the hydrology of the upper Mara River Basin, Kenya: results of a modeling study to support better resource management. Hydrol. Earth Syst. Sci. 15:2245–2258. https://doi.org/10.5194/hess-15-2245-2011.

Mann, H. B. (1945). Nonparametric tests against trend. Econometrica: Journal of the econometric society, 245-259.

Martin-Vide, J. (2004). Spatial distribution of a daily precipitation concentration index in peninsular Spain. International Journal of Climatology: A Journal of the Royal Meteorological Society, 24(8), 959-971.

Mengistu, K. T. (2009). Watershed hydrological responses to changes in land use and land cover, and management practices at Hare Watershed, Ethiopia.

Michiels, P., Gabriels, D., & Hartmann, R. (1992). Using the seasonal and temporal precipitation concentration index for characterizing the monthly rainfall distribution in Spain. Catena, 19(1), 43-58.

Mishra, V. N., Rai, P. K., & Mohan, K. (2014). Prediction of land use changes based on land change modeler (LCM) using remote sensing: a case study of Muzaffarpur (Bihar), India. Journal of the Geographical Institute" Jovan Cvijic", SASA, 64(1), 111-127.

Nash, J. E. & Sutcliffe, J. V. (1970) River flow forecasting through conceptual models. Part I—A discussion of principles. J. Hydrol. 27(3), 282–290.

Ndulue, E., & Mbajiorguu, C. (2019). Modeling climate and land-use change impacts on streamflow and sediment yield of an agricultural watershed using SWAT. Agricultural Engineering International: CIGR Journal, 20(4), 15-25.

Novotny, E. V., & Stefan, H. G. (2007). Stream flow in Minnesota: Indicator of climate change. Journal of Hydrology, 334(3-4), 319-333.

Orlandi, S., Probo, M., Sitzia, T., Trentanovi, G., Garbarino, M., Lombardi, G., & Lonati, M. (2016). Environmental and land use determinants of grassland patch diversity in the western and eastern Alps under agro-pastoral abandonment. Biodiversity and Conservation, 25(2), 275-293.

Pingale, S. M., Khare, D., Jat, M. K., & Adamowski, J. (2016). Trend analysis of climatic variables in an arid and semi-arid region of the Ajmer District, Rajasthan, India. Journal of Water and Land Development.

Romanowicz, R.J., Booij, M.J., 2011. Impact of land use and water management on hydrological processes under varying climatic conditions. Phys. Chem. Earth 36:613–614. https://doi.org/10.1016/j.pce.2011.08.009.

Rostamian, R., Jaleh, A., Afyuni, M., Mousavi, S. F., Heidarpour, M., Jalalian, A., & Abbaspour, K. C. (2008). Application of a SWAT model for estimating runoff and sediment in two mountainous basins in central Iran. Hydrological sciences journal, 53(5), 977-988.

Sanchez, L. A., Ataroff, M., & Lopez, R. (2002). Soil erosion under different vegetation covers in the Venezuelan Andes. Environmentalist, 22(2), 161-172.

Soil Conservation Service. (1972). National engineering handbook, section 4, hydrology.

Song, X., Song, S., Sun, W., Mu, X., Wang, S., Li, J., & Li, Y. (2015). Recent changes in extreme precipitation and drought over the Songhua River Basin, China, during 1960–2013. Atmospheric Research, 157, 137-152.Srinivasan, C. Santhi, R. Harmel, A. Van Griensven, M. W. Van Liew et al., "Swat: Model use, calibration, and validation," Transactions of the ASABE, vol. 55, no. 4, pp. 1491–1508, 2012.

Srinivasan, R., Ramanarayanan, T. S., Arnold, J. G., & Bednarz, S. T. (1998). Large area hydrologic modeling and assessment part II: model application 1. JAWRA Journal of the American Water Resources Association, 34(1), 91-101.

Tian, P., Lu, H., Feng, W., Guan, Y., & Xue, Y. (2020). Large decrease in streamflow and sediment load of Qinghai–Tibetan Plateau driven by future climate change: A case study in Lhasa River Basin. Catena, 187, 104340.

Trang, N. T. T., Shrestha, S., Shrestha, M., Datta, A., & Kawasaki, A. (2017). Evaluating the impacts of climate and land-use change on the hydrology and nutrient yield in a transboundary river basin: A case study in the 3S River Basin (Sekong, Sesan, and Srepok). Science of the Total Environment, 576, 586-598.

Veronez, M. R., Thum, A. B., Luz, A. S., & Da Silva, D. R. (2006). Artificial neural networks applied in the determination of soil surface temperature–SST. In International Symposium Accuracy Assessment in Natural Resources and Environmental Sciences,(Accuracy 2006) (Vol. 7, pp. 889-898).

Wang, J., Wang, K., Zhang, M., & Zhang, C. (2015). Impacts of climate change and human activities on vegetation cover in hilly southern China. Ecological engineering, 81, 451-461.

Williams, J. R., & Berndt, H. D. (1977). Sediment yield prediction based on watershed hydrology. Transactions of the ASAE, 20(6), 1100-1104.

Xu, B., Li, Y., Han, F., Zheng, Y., Ding, W., Zhang, C., ... & Zhang, Z. (2020). The transborder flux of phosphorus in the Lancang-Mekong River Basin: magnitude, patterns and impacts from the cascade hydropower dams in China. Journal of Hydrology, 590, 125201.

Xu, B., Li, Y., Han, F., Zheng, Y., Ding, W., Zhang, C., ... & Zhang, Z. (2020). The transborder flux of phosphorus in the Lancang-Mekong River Basin: magnitude, patterns and impacts from the cascade hydropower dams in China. Journal of Hydrology, 590, 125201.

Xu, X., Chen, H., & Levy, J. K. (2008). Spatiotemporal vegetation cover variations in the Qinghai-Tibet Plateau under global climate change. Chinese Science Bulletin, 53(6), 915-922.

Xu, X., Yang, D., Yang, H., & Lei, H. (2014). Attribution analysis based on the Budyko hypothesis for detecting the dominant cause of runoff decline in Haihe basin. Journal of Hydrology, 510, 530-540.

Yang, L., Feng, Q., Yin, Z., Deo, R. C., Wen, X., Si, J., & Li, C. (2017). Separation of the climatic and land cover impacts on the flow regime changes in two watersheds of Northeastern Tibetan Plateau. Advances in Meteorology, 2017.

Yesuf, H. M., Assen, M., Alamirew, T., & Melesse, A. M. (2015). Modeling of sediment yield in Maybar gauged watershed using SWAT, northeast Ethiopia. Catena, 127, 191-205.

Zarei, A., Asadi, E., Ebrahimi, A., Jafari, M., Malekian, A., Nasrabadi, H. M., ... & Maskell, G. (2020). Prediction of future grassland vegetation cover fluctuation under climate change scenarios. Ecological Indicators, 119, 106858.

Zhang, B., Ding, W., Xu, B., Wang, L., Li, Y., & Zhang, C. (2019). Spatial characteristics of total phosphorus loads from different sources in the Lancang River Basin. Science of the Total Environment, 722.https://doiorg.proxy2.library.illinois.edu/10.1016/j.scitotenv.2020.137863

Zhang, S., Li, Z., Lin, X., & Zhang, C. (2019). Assessment of climate change and associated vegetation cover change on watershed-scale runoff and sediment yield. Water (Switzerland), 11(7). https://doi-org.proxy2.library.illinois.edu/10.3390/w11071373

Zhang, X., Zwiers, F. W., & Li, G. (2004). Monte Carlo experiments on the detection of trends in extreme values. Journal of Climate, 17(10), 1945-1952.

Zhao, B., Zhang, L., Xia, Z., Xu, W., Xia, L., Liang, Y., & Xia, D. (2019). Effects of rainfall intensity and vegetation cover on erosion characteristics of a soil containing rock fragments slope. Advances in Civil Engineering, 2019.

Zheng, Y., Han, F., 2016. Markov Chain Monte Carlo (MCMC) uncertainty analysis for watershed water quality modeling and management. Stoch. Environ. Res. Risk A 30 (1), 293-308